Eur. J. Mech. B - Fluids 19 (2000) 575–595

S0997-7546(00)00122-9/FLA

Changing lift and drag by jet oscillation: experiments on a circular cylinder with turbulent separation

Jean-Christophe Béra *, Marc Michard, Michel Sunyach, Geneviève Comte-Bellot

Laboratoire de Mécanique des Fluides et d'Acoustique, UMR 5509, Mécanique des Fluides Active, GDR 1186, Ecole Centrale de Lyon – Centre Acoustique, 36 avenue Guy de Collongue, BP 163, 69131 Ecully cedex, France

(Received 28 April 1999; revised 23 July 1999; accepted 27 November 1999)

Abstract – Oscillating jet actuators have been implemented and tested on a circular cylinder. Their action on the separation of turbulent boundary layers is investigated using complementary approaches. Wall pressure distribution shows that a large lift is generated, at the expense, however, of a slightly increased drag. Particle image velocimetry measurements provide the mean and fluctuating velocity fields in the near-wake. The control jet deflects the mean flux lines towards the wall, illustrating that the separation is delayed. This effect appears more and more powerful as the pulsed jet velocity increases. Phase averaging of the PIV fields shows that periodic structures are generated by the control, and how these structures modify the aerodynamic forces by entraining the external flow towards the wall. Finally, a few comparisons are made with laminar boundary layers and some general mechanisms are presented for the lift increase. © 2000 Éditions scientifiques et médicales Elsevier SAS

control / cylinder wake / PIV / pulsed jet / separation

1. Introduction

It has been recently recognised that pulsed jets constitute an efficient way to modify the flow separation of bluff bodies. For airfoils, extensive experimental results have been obtained by Wygnanski [1] and his collaborators (Seifert et al. [2], Greenblatt et al. [3]) and by McManus et al. [4]. For circular cylinders, investigations have been performed by Amitay et al. [5] and Béra and Sunyach [6]. The pulsed jet technique also increases the lift coefficient significantly. Measurements of the mean wall pressure distribution around a circular cylinder by Béra et al. [7] have provided quantitative results on the lift gain.

So far, the case of laminar separation has been mostly widely investigated. In that situation, the physical mechanism invoked for the wake transformation is that the jet oscillations perturb the boundary layer so as to provoke its transition.

At higher speeds, when transition and turbulent separation occur, preliminary experiments by Amitay et al. [5] or by Béra et al. [7] have shown that a gain in lift can be also realised. The exact physical mechanism which takes place has, however, not yet been established, so that there is a need for having more experimental data concerning the flow response and its subsequent evolution.

The present study has been conducted in order to describe the interaction of an oscillating jet with the whole flow environment. The basic case of the circular cylinder has been retained. The experiments were conducted at a Reynolds number of $\mathrm{Re}_D = \frac{U_\infty D}{\nu} = 1.33 \cdot 10^5$ with tripped boundary layers. Several data sets have been collected so as to perform a global analysis of the flow. Firstly, the mean wall pressure distribution provides the aerodynamic global effects such as changes in lift and drag. The fluctuating part of the pressure is also worth

* Correspondence and reprints; e-mail: Jean-Christophe.Bera@ec-lyon.fr

studying, as it provides information on how strong and how close to the cylinder the energetic flow structures occur. Secondly, the velocity field is explored by Particle Image Velocimetry which is very appropriate to the situation where large unsteady velocity fields have to be analysed. The averages of random snapshots determine the mean wake modifications. Conditional averages with the phase of the pulsating jets were also conducted so as to determine the most coherent part of the controlled flow.

2. Experimental set-up

2.1. Wind tunnel and cylinder

The experiments were conducted in a wind tunnel on a circular cylinder. The cylinder diameter was $D = 10$ cm, and the tunnel section was square (40 cm $\times$ 40 cm). The incoming mean velocity was fixed at $U_\infty = 20$ m/s, with a residual turbulence intensity less than 0.3%. At the Reynolds number considered, $\mathrm{Re}_D = 1.33 \cdot 10^5$, the boundary layers on the cylinder are naturally laminar. Two trip wires (diameter 2 mm) were therefore placed at $\pm 28°$ from the front stagnation point to force boundary layer transition, as in previous works [6,7]. The turbulent nature of the boundary layer was globally checked by the pressure distribution around the cylinder as reported by Achenbach [8]. The jet oscillation actuator slit was set at 110° from the stagnation point. *Figure 1* is a schematic diagram of the experimental set-up. The position of 110° has been shown to be the most efficient one to create lift, as reported by Béra and Sunyach [6].

2.2. Jet oscillation actuator

2.2.1. Actuator design

The jet oscillation actuator is based on a pulsed cavity coupled with the external flow through a thin slit on the bluff body's wall, as sketched in *figure 2*. The injector slit is perpendicular to the wall, its width in the streamwise direction is 1 mm, and its length along the cylinder span is 10 cm. The slit was centred on the mid-span region of the cylinder. The pressure fluctuations in the cavity were generated by an electrodynamic acoustic source, and thus a large range of pressure amplitudes and frequencies can be monitored. A convergent nozzle connects the circular acoustic source to the slit. These fluctuations induce an alternating flow through the slit, with zero net mass flux.

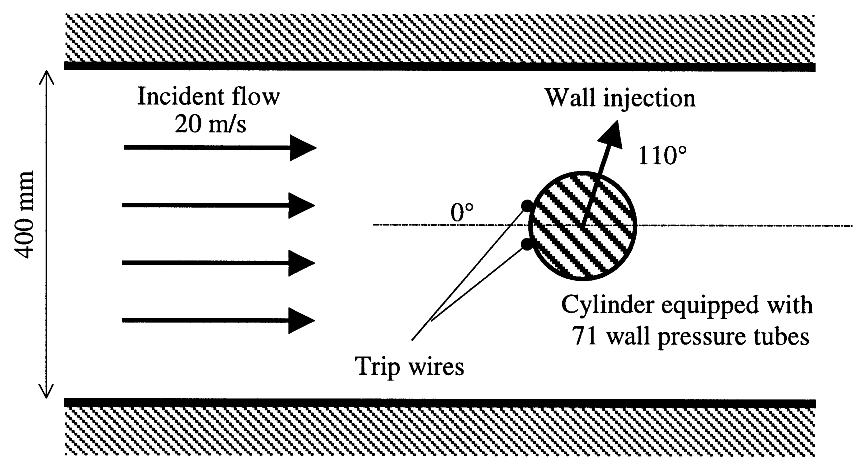

Figure 1. Experimental set-up.

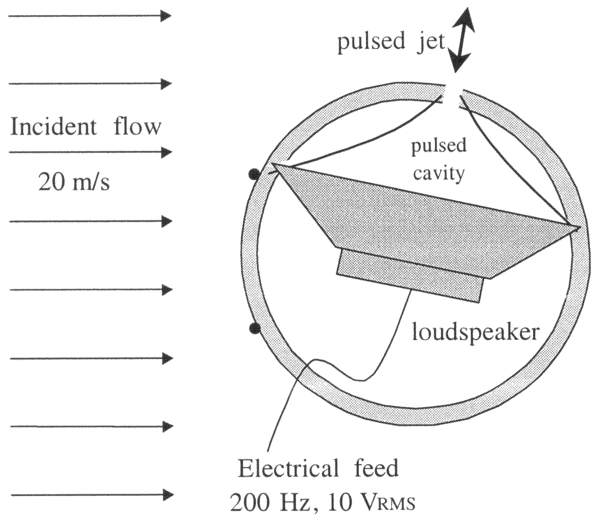

Figure 2. Principle of the pulsed jet actuator.

2.2.2. Jet oscillation characterisation

The electric feed on the actuator was a $f = 200$ Hz sine signal, giving a Strouhal number of $St = \frac{fD}{U_\infty} = 1$. This frequency is in the middle of the frequency range where the control jet has been observed to be active for lift generation [1,4]. The vertical velocity of the jet oscillation was characterised in the absence of external flow using a one-component laser Doppler anemometer. 50 000 Doppler signals were acquired at random times, along with a reference signal synchronised with the electrical feed of the actuator. The phase position of every Doppler signal was therefore known within the actuator cycle. The data were then accumulated for each phase position in the cycle, permitting statistical phase averages to be obtained. The precision in the phase allotment is around 0.7°.

Figure 3 indicates the vertical phase-averaged mean velocities obtained at 0.25 mm above the slit in the median plane, for a complete cycle of the actuator. The oscillation amplitude of the jet flux is clearly linked to the electrical feed amplitude. The mean value over an injection cycle is, however, not zero, because of the distinct flow patterns associated with the blowing and suction phases. Particle image velocimetry that was recently performed in the slit vicinity [9] shows that the blowing phase gives nearly straight outwards velocities, like a classical steady jet, while the flow induced by the suction is omnidirectional. As a result, the vertical velocity is larger during blowing than during suction. In addition, the flow is very smooth during suction and irregular during blowing.

The results we present in the following sections concern the flow obtained around the cylinder in four cases: without control, and with three actuator levels, corresponding to peak jet velocities near the slot exit of 22, 31 and 42 m/s. Compared to the free-stream velocity, the explored jet velocity range is 1.1 to 2.1. The two extreme cases of 22 m/s and 42 m/s were the most extensively investigated. In short, these two velocity amplitudes will be referred to as low- and high-level control, respectively.

2.3. Measurement techniques

2.3.1. Wall pressure measurements

The cylinder is equipped with 71 pressure ports, equally spaced around the circumference, every 5°. A scanning-valve system connected to the computer-based data acquisition system monitored the pressure

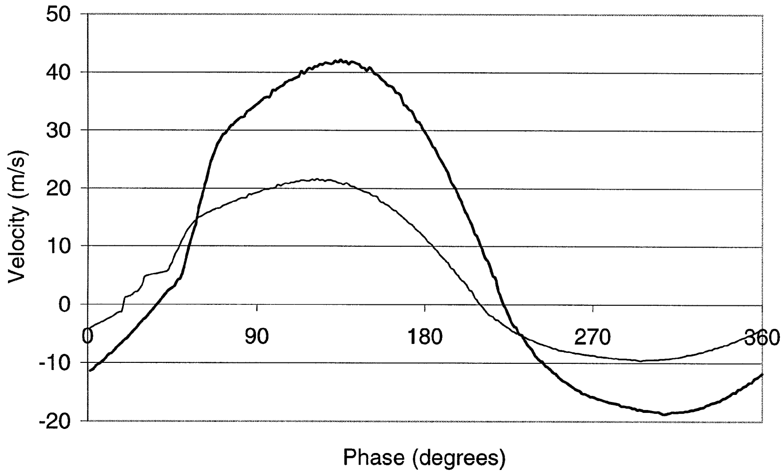

Figure 3. Phase-average vertical velocity cycle without external flow: for the high-level pulsed jet (thick line); for the low-level pulsed jet (thin line). (Velocity measured by laser Doppler anemometry at 0.25 mm above the slit on the jet axis, phase referred to the sine electrical feed.)

signals on a differential manometer. This provided the mean pressure distribution around the cylinder, which gives, by integration, the form drag and lift coefficients. A B & K microphone probe was also connected to the measurements ports to analyse the wall pressure fluctuations. Including the connection pipe, the frequency band was $40-10000$ Hz.

2.3.2. *Velocity field measurements*

Instantaneous velocity fields were measured by the particle image velocimetry technique (PIV). The flow was seeded with small oil droplets of approximately 1 to 2 μm in diameter, generated by a smog generator located at the inlet of the wind tunnel fan. The measurement of the particle velocity was based on two coupled YAG laser sources, where the time delay between two pulses was 15 μs. The light scattered by the seeding particles was recorded with a 1008×1018-pixels Kodak Megaplus ES-1–0 CCD camera. The lasers and the camera were synchronised with a commercial Dantec system. Pairs of raw images were cross-correlated using 32×32-pixels interrogation windows, with a 50% overlap ratio between adjacent windows. The size of the field of view was nearly 65×65 mm (magnification ratio of image/object $\approx 1/6$). The resulting spatial resolution of the PIV measurement is approximately 2 mm $\times$ 2 mm. Although the spatial resolution is not small compared to the slit width, the global flow structure induced by the jet oscillations in the whole near-wake is correctly resolved. The data validation is performed by a dynamic procedure using 8 neighbouring points, Raffel et al. [10].

The measurement mode was a either 'free run', at the natural repetitive frequency of the YAG laser (nearly 9 Hz), or triggered by the PC signal imposing a phase within the injection cycle. The phase delay was adjustable by steps of 20°. Ensemble averages are obtained on 900 free-run instantaneous fields in the former case, and on 50 triggered instantaneous fields for each phase in the latter case. We have verified that the mean over the 18 phase delays of these 18×50 triggered fields is consistent with the ensemble average over the free runs.

2.4. *Post-processing of PIV data*

2.4.1. *Eddy localisation technique*

The criterion developed by Michard et al. [11] was used to locate the vortex centres. It is based on a normalised angular momentum, rather than on differential operators as in Raffel et al. [10]. A dimensionless

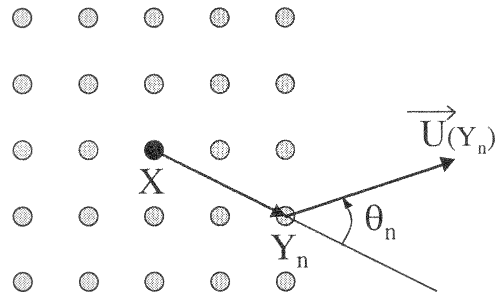

Figure 4. Integration domain for the vortex Γ-criterion calculation at any point X.

function $\Gamma(\vec{X})$ is defined at every point $\vec{X}$ of the velocity field by:

$$\Gamma(\vec{X}) = \frac{1}{N}\sum_{n=1}^{N}\frac{\|(\vec{Y}_n - \vec{X}) \wedge \vec{U}_n\|}{\|\vec{Y}_n - \vec{X}\|\,\|\vec{U}_n\|} = \frac{1}{N}\sum_{n=1}^{N}\sin\theta_n$$

where $\vec{Y}_n$ are the $N = 24$ neighbours of $\vec{X}$ over a 5×5 square domain, and θ_n the angle between the relative position vector $\vec{Y}_n - \vec{X}$ and the velocity vector $\vec{U}(\vec{Y}_n)$, see *figure 4*. Each point of the 5×5 square domain corresponds to a PIV interrogation window. The whole flow field is analysed with an interrogation window overlap of 75%. The vortex centre positions $\vec{X}$ are given by the extrema of $\Gamma(\vec{X})$ when they are close to 1 or -1. A positive value of $\Gamma(\vec{X})$ corresponds to a counter clockwise rotation and a negative value of $\Gamma(\vec{X})$ to a clockwise rotation. The spatial detection scale, which is linked to the size of the 5×5 integration domain, is adjusted to remove local turbulent fluctuations and measurements errors, e.g. subpixel interpolation for PIV measurements.

2.4.2. Proper Orthogonal Decomposition

The Proper Orthogonal Decomposition (POD) was applied to the fluctuations of an ensemble of triggered velocity fields at a given phase. We used the snapshot technique which reduces the computational cost of the eigenvalues problem to be solved, see Holmes et al. [12], Graftieaux [13]. At a given phase, the set of fluctuating snapshots is obtained by removing, from every field, the phase-averaged velocity field which corresponds to that phase. The eigenvalues, λ_j, of the correlation matrix deduced from this set of snapshots are computed as well as the corresponding eigenmodes from which an orthonormal basis of spatial modes is derived. Each snapshot is then projected on this basis. For a given spatial mode, of order j, the variance of the corresponding coefficient of projection is equal to λ_j. Therefore, λ_j indicates the kinetic energy associated to the spatial mode j over the whole domain. The spatial structure of the corresponding mode shows where these fluctuations take place in the measurement domain. In the following, we focus our attention mainly on the most energetic mode of the projection. At every phase, we have used 50 snapshots.

3. Wall pressure results

3.1. Lift and drag global effects

The global aerodynamic effect on the cylinder of the control jet, in terms of lift and drag, is presented in *figure 5*. The lift increase is particularly important. It is measured with respect to the lift coefficient without

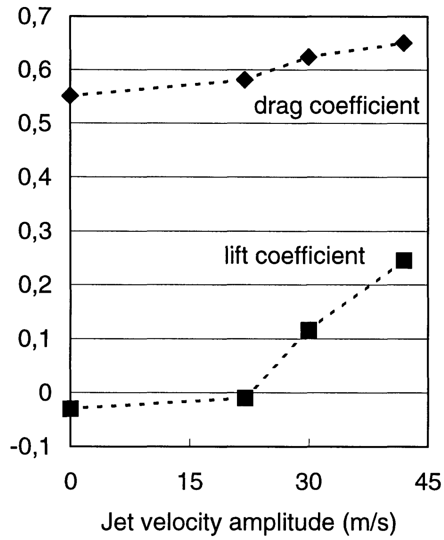

Figure 5. Form drag and lift coefficients as a function of the velocity amplitude at the injector exit, in the case of turbulent boundary layer separation.

control, which is not exactly zero, because of minor flow asymmetries in the experimental set-up (position of trip-wires, presence of the slit opening). The jet oscillations generate a lift force, which increases with the control jet amplitude. This increase is non-linear; while a very small effect is registered at low-level control (22 m/s), a very large lift force occurs at high-level control (42 m/s) with a gain in lift coefficient of 0.24. For an intermediate jet velocity (31 m/s), an intermediate lift value is obtained, which demonstrates that the physical mechanism involved is progressive.

The drag is also affected by the control, but only slightly. Without jet oscillation, the drag coefficient is low, about 0.55, corresponding to the turbulent separation of the boundary layer. With control, the drag coefficient becomes 0.65 for the high-level control (42 m/s). These results, as well as the lift generation, are in good agreement with the previous experiments on turbulent separation control [7].

As a comparison, the control in the case of laminar boundary layer separation was carried out using the same experimental conditions, but without the trip wires. *Figure 6* shows that the control generates a substantial lift and has a very low effect on drag. This behaviour is associated with a boundary layer excitation resulting in a downstream shift of the separation point with the control. Compared to previous measurements on cylinders [5,7], the effect of the present control is slightly reduced. The reason is that in the present study the azimuthal position of the control jet, 110°, differs from the optimal control position for the laminar case, 90°, as described by Béra and Sunyach [6]. However, it is particularly interesting to point out that an oscillation control at 110° is still acting in the laminar separation case.

3.2. Mean pressure distributions over the cylinder

The wall pressure behaviour is depicted in *figure 7*. Without control, the natural separation occurs at about $\pm 110°$ azimuth. It is preceded by a suction area and followed by a large zone of uniform low negative pressure. Compared with Achenbach [8], this pressure distribution corresponds to an effective Reynolds number of about $5 \cdot 10^5$. Such an increase above the geometrical Reynolds number $\mathrm{Re}_D = \frac{U_\infty D}{\nu} = 1.33 \cdot 10^5$ is due to the strong turbulence created by the trip wires. When the control is on, the jet oscillations act on a large azimuthal range

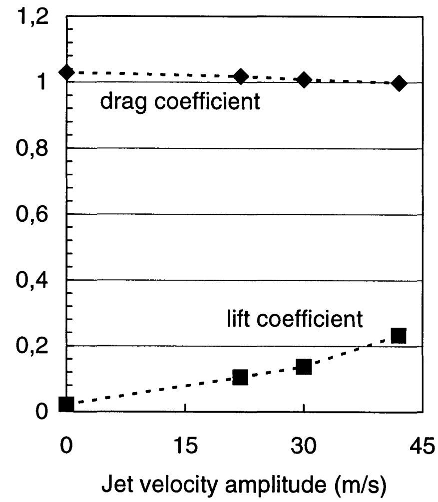

Figure 6. Form drag and lift coefficients as a function of the velocity amplitude at the injector exit, in the case of laminar boundary layer separation.

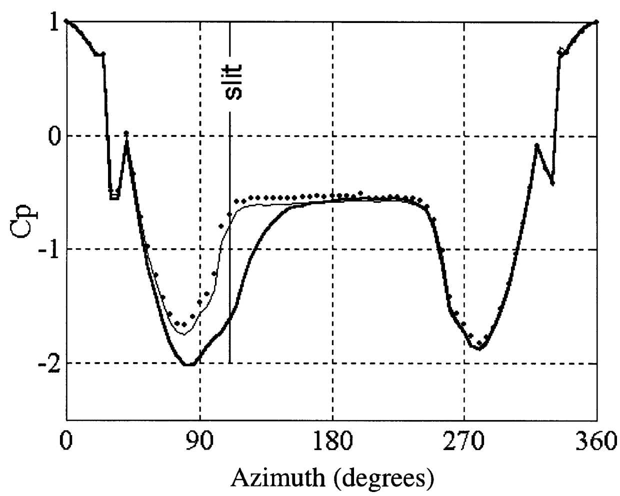

Figure 7. Wall pressure distribution in the case of turbulent boundary layer separation without control (dotted line), with the low-level pulsed jet (thin line), and with the high-level pulsed jet (thick line).

$(50° - 180°)$. The suction profile has an increased depth, so that higher negative pressures are generated on the upper part of the cylinder, leading to a substantial lift increase.

The azimuthal zone $180° - 360°$ is virtually unaffected by the control. This is due to 3-D flows occurring near the ends of the 10 cm slit in the present experiments. Indeed, additional experiments in progress with a 20 cm slit show that the control possibly affects the pressure distributions in the $180° - 360°$ region. Also numerical predictions in a pure 2D case – corresponding to the slit spanning the entire length of the cylinder – clearly lead to a global flow response around the cylinder, Getin [14].

As a comparison, *figure 8* shows the wall pressure distribution around the cylinder with and without the jet oscillation in the case of laminar separation conditions. Without control, a small uniform suction area exists between the two separation points located at 85° and 275°. When the control jet is operating, being still located at 110°, a pressure dip is created in the azimuthal range $70° - 150°$. The controlled pattern in the laminar case

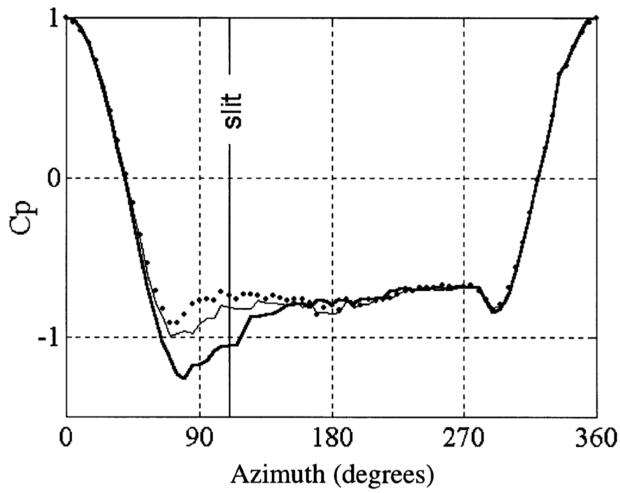

Figure 8. Wall pressure distribution in the case of natural laminar boundary layer separation without control (dotted line), with the low-level pulsed jet (thin line), and with the high-level pulsed jet (thick line).

is somewhat similar to the case of turbulent boundary layer separation, although the suction remains moderate. This suggests that a partial transition occurs, compared to the full transition observed by Béra and Sunyach [6] with the optimal position of 90°. Nevertheless, this shows that it is possible to control laminar separation even when the control jet acts 25° downstream of the natural separation point.

3.3. Wall pressure fluctuations

Two azimuths, 105° and 115°, are selected in *figures 9* and *10*. They are on either side of the control slit located at 110°. In the absence of control, the natural vortex shedding imposes its structure on the wake. The wall trace of this structure is clearly visible on the wall pressure spectra, around 50 Hz. More frequency-accurate measurements showed a bump at 52 Hz, hence $St = 0.26$. The bump – instead of a peak – corresponds to a mean observation of a fluctuating Strouhal. Taking into account that the effective Reynolds number is around $5 \cdot 10^5$ in our experiments, the Strouhal value of 0.26 is indeed in the range classically obtained at critical Reynolds numbers, Blake [15]. As a final comment, it is interesting to note that at 115°, the wall pressure spectra possess very little high frequency contributions, although the natural separation point without forcing occurs around 110°. The reason is that the eddies leaving the cylinder and constituting later on the separated free shear layer, stay away from the wall so that their distant influence does not reach the wall.

When the control is on, the natural Strouhal bump disappears. It is replaced by a series of discrete peaks at the frequency of the control jet and its harmonics. The harmonics simply express the fact that the control jet has a more complex form than a sine oscillation as explained in section 2.2.2. Interestingly, the high frequency contents of the wall pressure spectra at 115°, downstream of the injection slit, have now recovered the high levels observed upstream of the injector slit at 105°. This is a convincing suggestion that the flow now remains attached to the wall, carrying with it the remnants of the synchronised structures created by the control jet near the slot. The PIV pictures confirm that assessment, as presented in section 4. As a consequence too, the separation is not yet attained at the azimuth 115°. Other measurements – not reported in the present study – indicate that the separation seems to occur near 140°.

The circumferential coherence of the wall pressure field is another way to look at the flow getting closer to the wall. Experiments have been carried out between the azimuths 115° and 140° and the results reported in

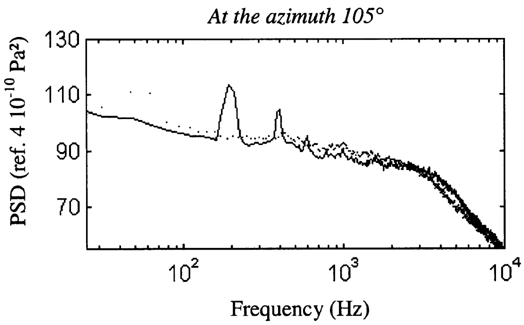

Figure 9. Wall pressure fluctuation spectrum at 5° upstream of the injection slit without control (dotted line) and with the high-level pulsed jet (continuous line).

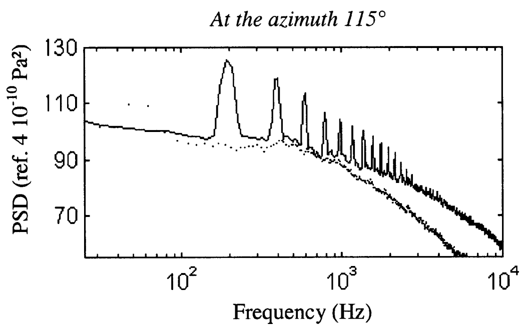

Figure 10. Wall pressure fluctuation spectrum at 5° downstream of the injection slit without control (dotted line) and with the high-level pulsed jet (continuous line).

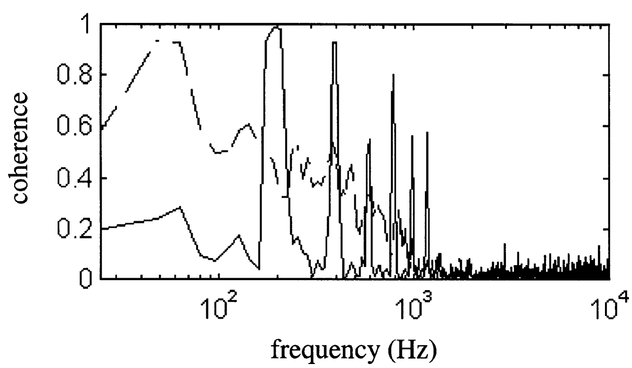

Figure 11. Coherence function of the wall pressure fluctuations between the azimuths 115° and 140°: without control (dotted line) and with the high-level pulsed jet (continuous line).

figure 11. Without control, the coherence is greater than 0.9 at the natural Strouhal frequency, and secondary maxima with decreasing amplitudes are observable at its harmonics. For the other frequencies, no significant coherence exists. Now, with control, a strong coherence appears, with levels in the range 0.6 – 0.9, for the frequency of the jet control and its harmonics. This clearly confirms that the structures created by the jet control are well organised and close to the wall. The flow is therefore attached to the wall up to at least the azimuth 140°. Thus the separation is substantially delayed.

4. Mean wake characterisation

4.1. Mean PIV velocity fields

Figures 12(a) to *12(c)* show how the mean velocity is highly modified by the pulsed jet. Without control, *figure 12(a)*, a large area of low mean velocity behind the cylinder is largely filled with reverse flow. The

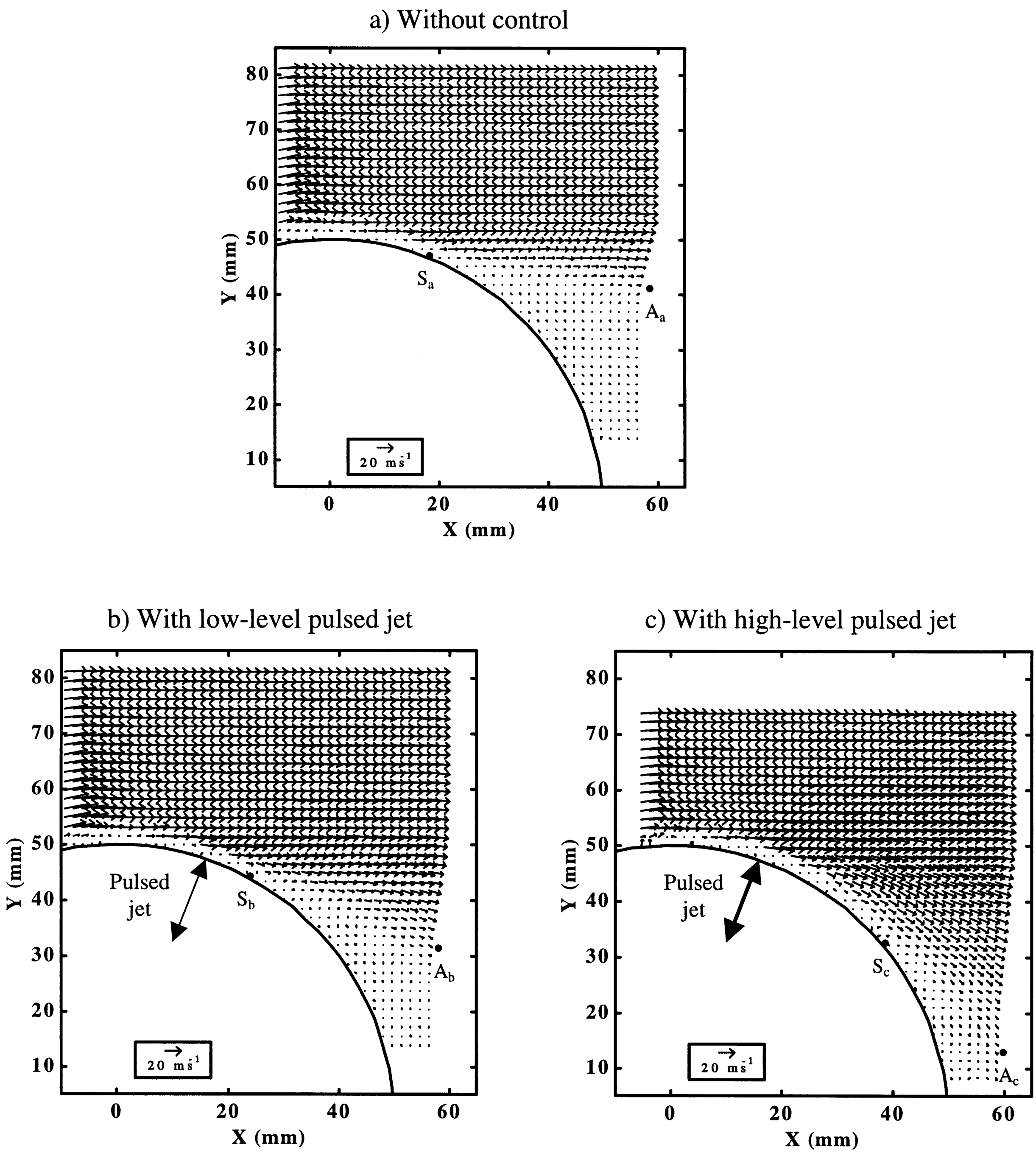

Figure 12. Mean velocity fields without (a) and with control (b) and (c). The estimated separation point is noted, S, and the separation line is SA.

shear layer which delimits this zone is clearly visible. Its lower boundary goes towards point A_a and defines a separation angle of approximately 8° with the upstream velocity. At the cylinder wall, the point of separation S_a is estimated at $X = 18$ mm, $Y = 48$ mm, hence about azimuth 110°, to within the size of one interrogation window of the PIV.

With the low-level pulsating jet, see *figure 12(b)*, the reverse flow area is reduced, its frontier pushed down, towards point A_b. The fluid from the upper part is also displaced downward. The separation angle can now be estimated at 18°, and at the cylinder wall the separation is located around $X = 25$ mm, $Y = 45$ mm, point S_b, hence about azimuth 120°.

With the high-level pulsating jet, see *figure 12(c)*, the mean flow remains clearly attached to the wall up to at least point S_c (azimuth 135°, $X = 38$ mm, $Y = 32$ mm). The separation angle is brought up to 45°. Accordingly, the reverse flow region has almost disappeared and a large downwards engulfing flow motion takes place behind the cylinder.

As an additional remark, the transverse mean velocity gradient becomes smaller and the shear layer wider, as shown by the downward displacement of point A from A_a to A_c.

4.2. Mean kinetic energy of the fluctuating velocity fields

The iso-contours of the mean kinetic energy of the velocity fluctuations are plotted, in *figure 13(a)* without control, *figure 13(b)* for the low-level control, and *figure 13(c)* for the high-level control. The highest values, which correspond to the most intense shear regions, clearly depict the downward displacement of the separated zone. Separation angles of 5°, 15°, and 40° are now estimated with no control, low- and high-level control, respectively. These values are very close to those estimated from the mean velocity fields.

Furthermore, when the control is on, the pulsed jets generate strong velocity fluctuations downstream of the injector. They are close to the wall and permit these synchronised structures to be detected by the fluctuating wall pressure measurements.

The relatively large kinetic energy levels that can be observed in the whole region between the smooth external flow and the delayed attached region near the cylinder, are due to the velocity fluctuations associated with the engulfed fluid motion. Expressed relatively to the free stream, intensities are around 12%.

Near the cylinder's rear, oscillations are detected as expected. They correspond to an alternately up and down motion. They appear to be strongest with the high-level control when the velocity close to the wall is largest.

5. Identification of the active eddy structures

5.1. Instantaneous eddies patterns

All the instantaneous fields presented in this section give the eddy centre Γ-criterion results, in colours, and the velocity vectors, with arrows. We recall that clockwise eddies are marked in blue.

5.1.1. Instantaneous fields without control

In *figure 14*, we give two representative examples of the field without control. We can observe the large undulations of the free shear layer, and just underneath well defined small clockwise eddies. These small eddies look similar to those observed by Prasad and Williamson [16] using a smoke wire to visualise the inner part of the separated layer of a cylinder. They attributed these small eddies to the most amplified frequencies f_{SL} of the shear layer instabilities and connected f_{SL} to the von Karman frequency f_K of the vortex shedding by the empirical relation $f_{SL}/f_K \approx 0.0235\,\mathrm{Re}_{\mathrm{D}}^{0.67}$. Now, let us try to estimate f_{SL} in our experiment. From the left

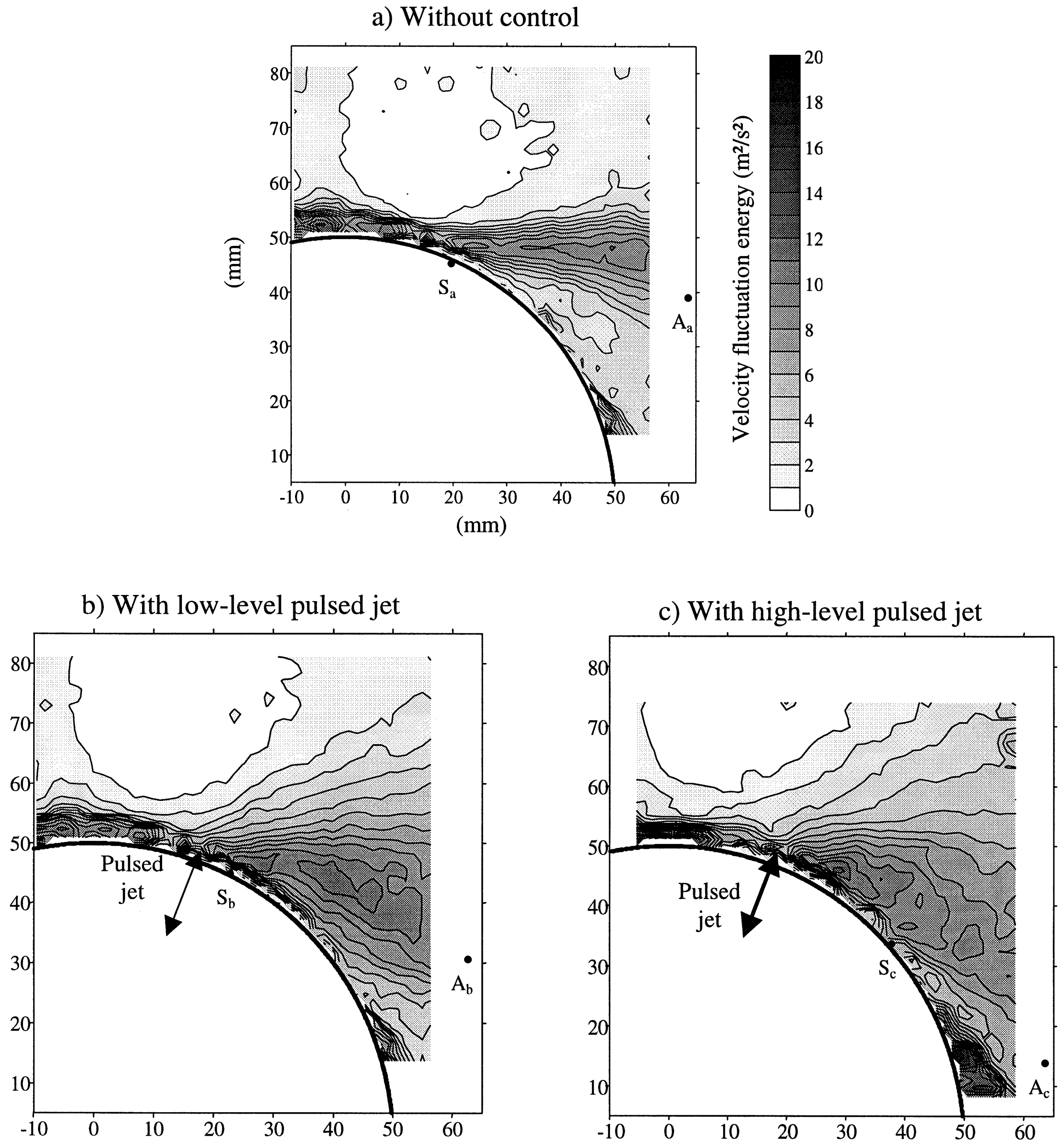

Figure 13. Kinetic energy of velocity fluctuation without (a) and with control (b) and (c).

picture of *figure 14* where at least two structures occur in the same picture, we deduce an occurrence frequency of the convected structures. Assuming a spatial separation (around 5 mm) and a convection velocity (around 10 m/s), we obtain a frequency f_{SL} of the order of 2 kHz. From the Prasad and Williamson formula, having in our experiments $f_K = 52$ Hz and $\mathrm{Re}_D = 1.33 \cdot 10^5$, we obtain $f_{SL} \approx 3$ kHz, which is of the order of the 2 kHz experimental value. The difference can be attributed to the fact that our Reynolds number is larger than the maximal one used by Prasad and Williamson and that transition has already taken place in our case.

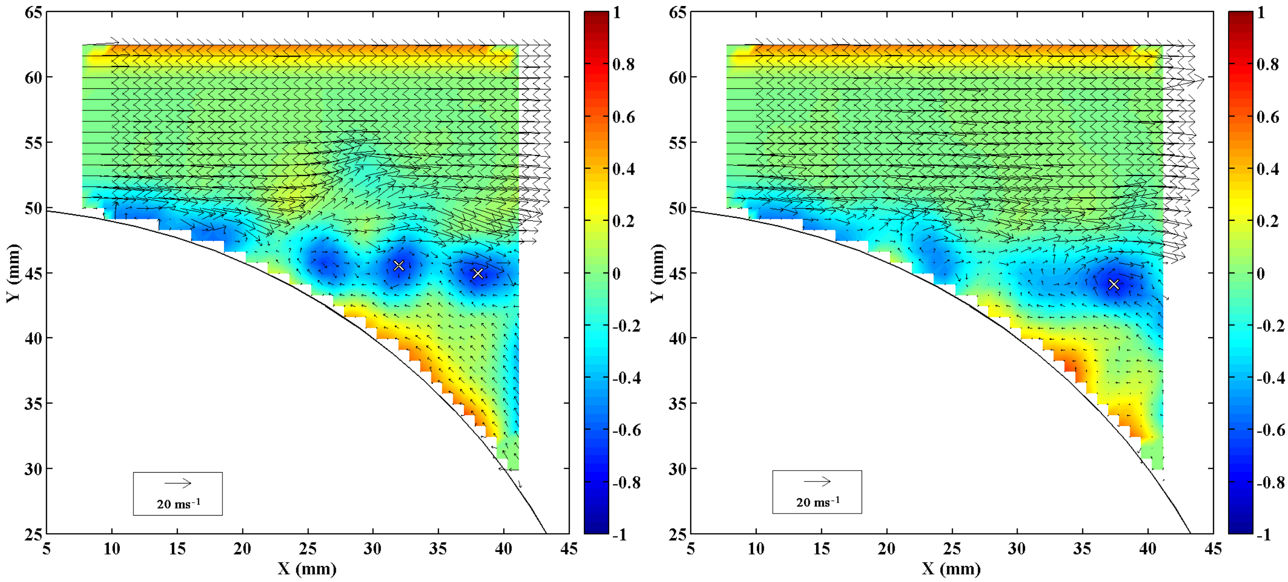

Figure 14. Without control, examples of instantaneous velocity fields (vectors) and eddy center Γ-criterion fields (colours).

5.1.2. Instantaneous fields with low- and high-level control

At this point, and because of the estimate which precedes, let us remark that the control frequency, $f = 200$ Hz, we have chosen as the most efficient one is located between the two widely separated frequencies f_K and f_{SL} , as f is around $4f_K$ and $f_{SL}/10$. This large difference motivates us to find another explanation than just a stability analysis to explain the way the separation control works. This is the main reason for the extended survey undertaken on the velocity field.

In *figures 15* and *16*, we present examples of the instantaneous fields obtained at two significant instants, or phases, of the injection cycle: 180° at the end of the blowing, and 0° at the end of the aspiration, see *figure 3*. Several results can be listed for the phase 180° (*figure 15*):

(i) there is always a well organised flow pattern in the vicinity of the slit – downstream of it as expected. This is due to the timing we imposed for looking at the fields. This pattern is not exactly at the same place on every realisation, because of the flow irregularities existing in the jet itself (the flow seems very smooth during suction, and irregular during blowing [9]) and the additional irregularities coming from its interaction with an incident turbulent boundary layer;

(ii) there is sometimes a similar pattern, but more blurred, farther downstream and close to the wall. This is the remnant of a preceding active structure, initiated 1/200 s, i.e. 5 ms earlier. When these are observable at the bottom right of the PIV picture, a convection speed can be estimated, using a travel difference (around 40 mm) and the available travel time (5 ms), so that the convection speed is around 8 m/s. Of course, this value is some sort of average during the structure motion, because we have not looked at the structure the whole time. During its motion, the structure might have moved faster or slower at some instants that we cannot precisely identify. Anyway, it is interesting to know that large velocities can exist close to the cylinder wall when the control is on. Also, the circumferential wall pressure coherence, which is advantageously deduced from continuous time pressure signals, is on its own a good indicator for organised structures existing and moving close to the wall;

(iii) all the eddies are clockwise – marked by negative values of the Γ-criterion – because they are not destroyed by the mean velocity gradient of the boundary layer. On the contrary, the counter clockwise

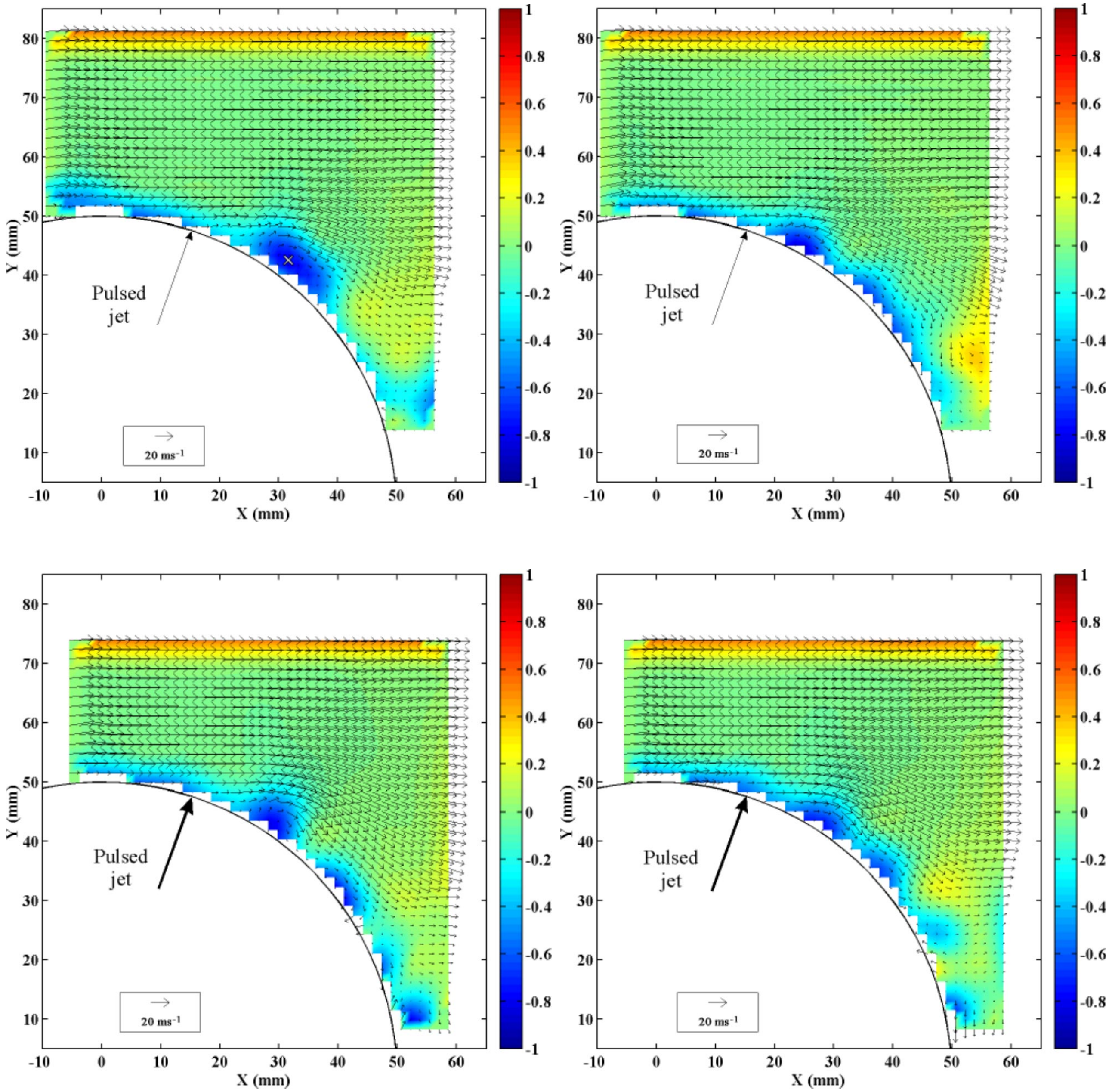

(a) (b)

Figure 15. With control, examples taken at the same injection cycle phase of 180° of instantaneous velocity fields (vectors) and eddy center Γ-criterion fields (colours): (a) low-level pulsed jet, (b) high-level pulsed jet.

eddies which obviously exist just at the slit exit without external flow [9], are immediately suppressed. The existence of only clockwise eddies are of primordial importance in the control mechanism of the turbulent boundary layer separation. These structures, and only these, can bring the flow close to the cylinder wall.

Figure 16 deals with the phase 0°, near the end of the aspiration. Three results can be listed:

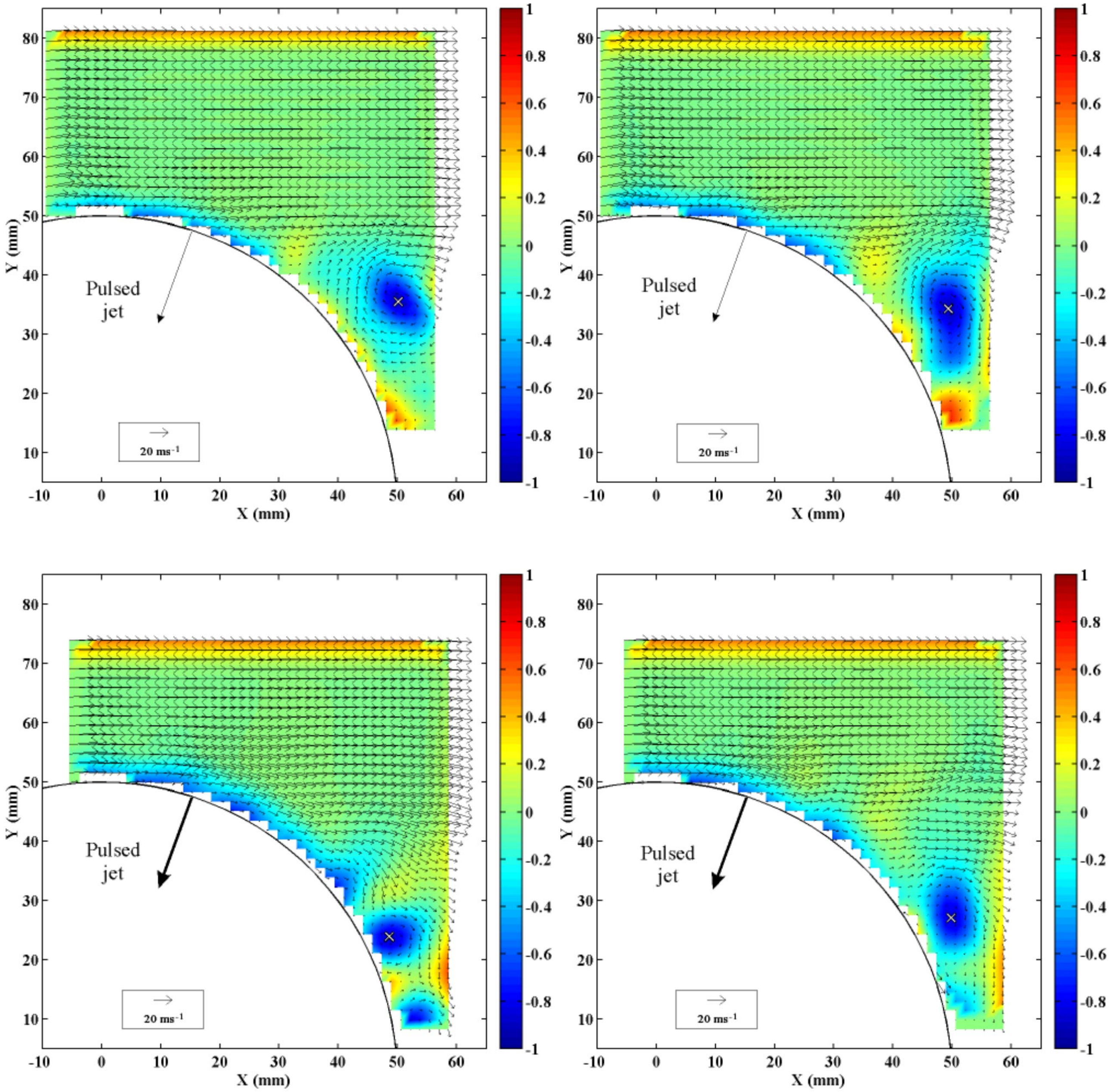

(a) (b)

Figure 16. With control, examples taken at the same injection cycle phase of 0° of instantaneous velocity fields (vectors) and eddy center Γ -criterion fields (colours): (a) low-level pulsed jet, (b) high-level pulsed jet.

(i) only one clockwise vortex structure is generally observed per realisation. The reason is that the structure we are looking at comes from the clockwise vortex which was generated during the preceding blowing period;

(ii) this structure is necessarily located farther downstream of the slit. It is remarkable that it has achieved a large displacement, around 30 mm;

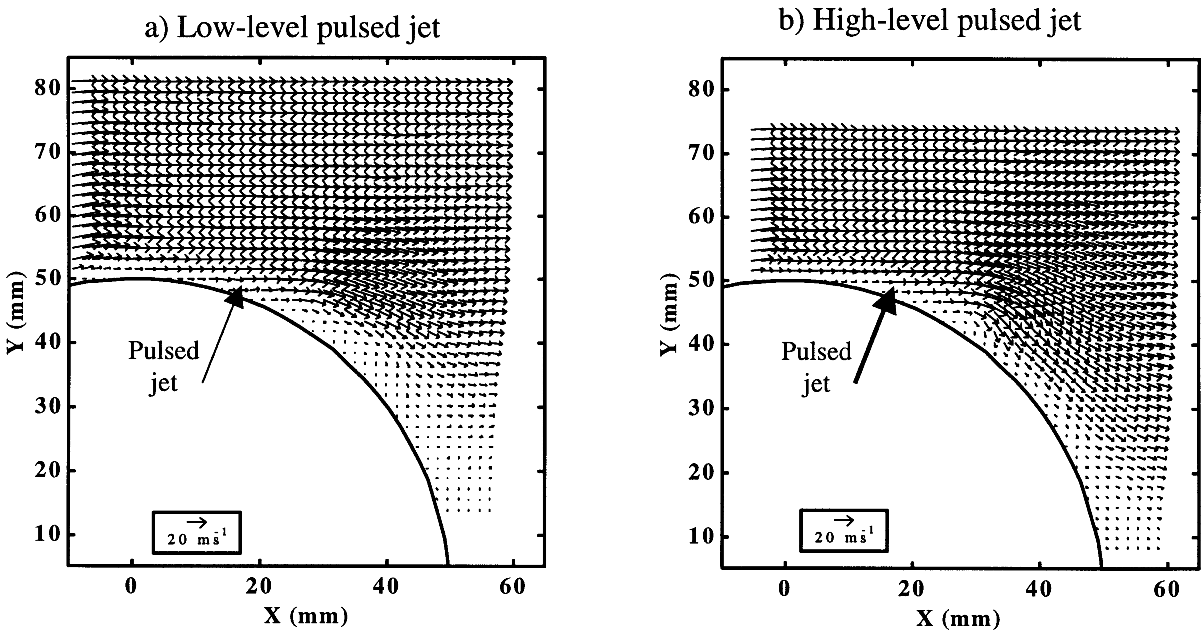

Figure 17. Phase-average velocity fields at the end of the blowing phase of the pulsed injection (180°) for low and high pulsed jet velocity amplitudes.

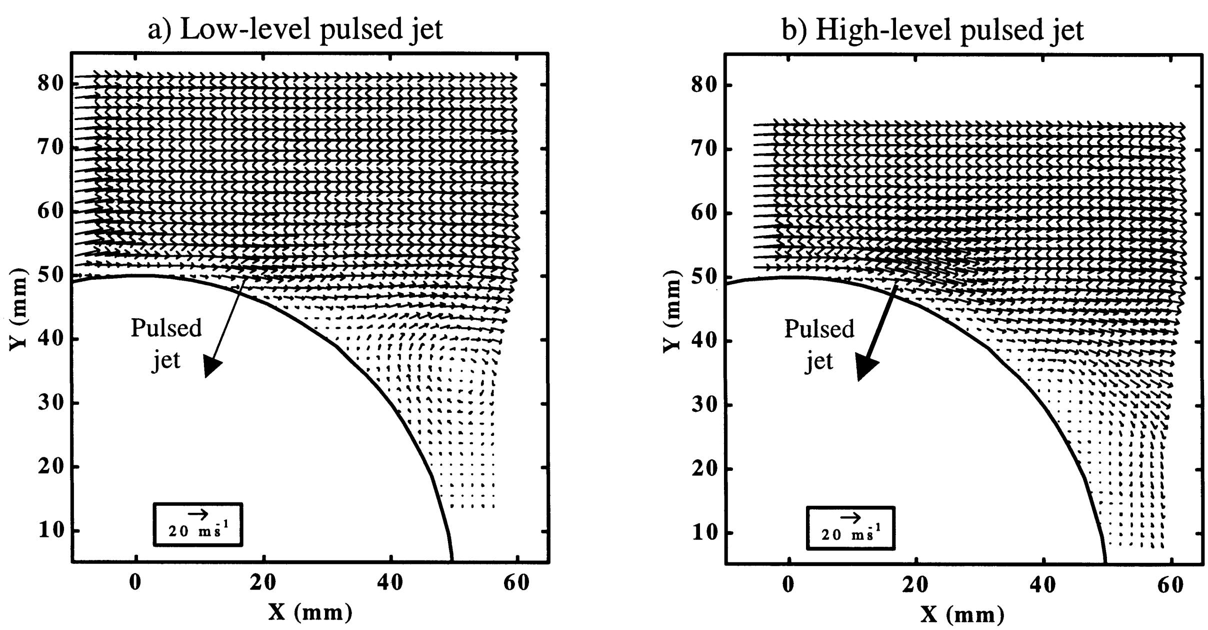

Figure 18. Phase-average velocity fields at the end of the aspiration phase of the pulsed injection (0°) for low and high pulsed jet velocity amplitudes.

(iii) this structure appears to be large, strongly organised, and gets closer to the wall when the control level increases. This specific feature is due to the initial clockwise motion of the vortex. Later on, this clockwise motion is even reinforced by the suction which takes place along the wall towards the slit, during the aspiration phase of the control jet.

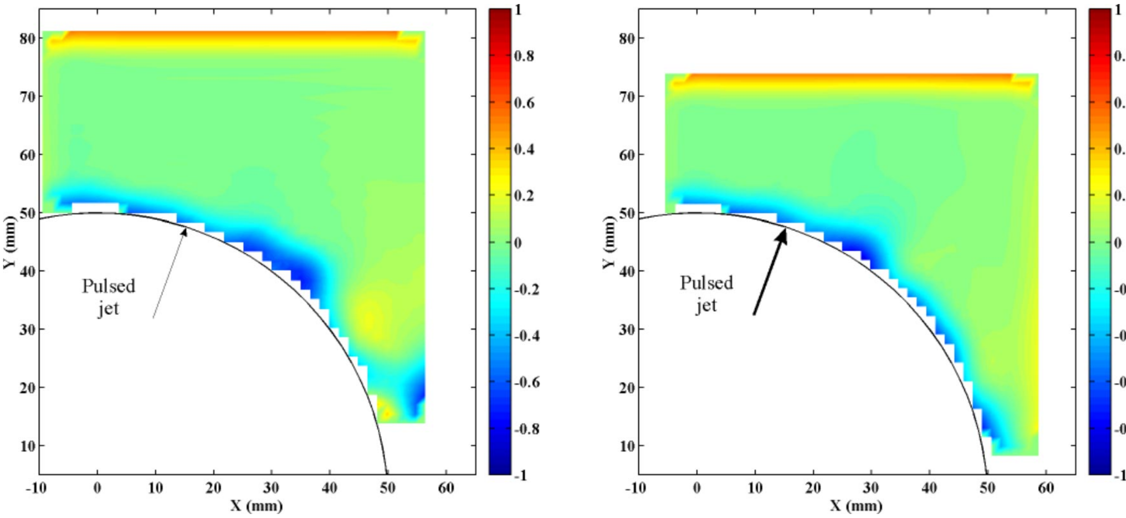

(a) (b)

Figure 19. Phase average fields of eddy center Γ-criterion at the end of the blowing phase of the pulsed injection (180°). (a) Low-level pulsed jet; (b) High-level pulsed jet.

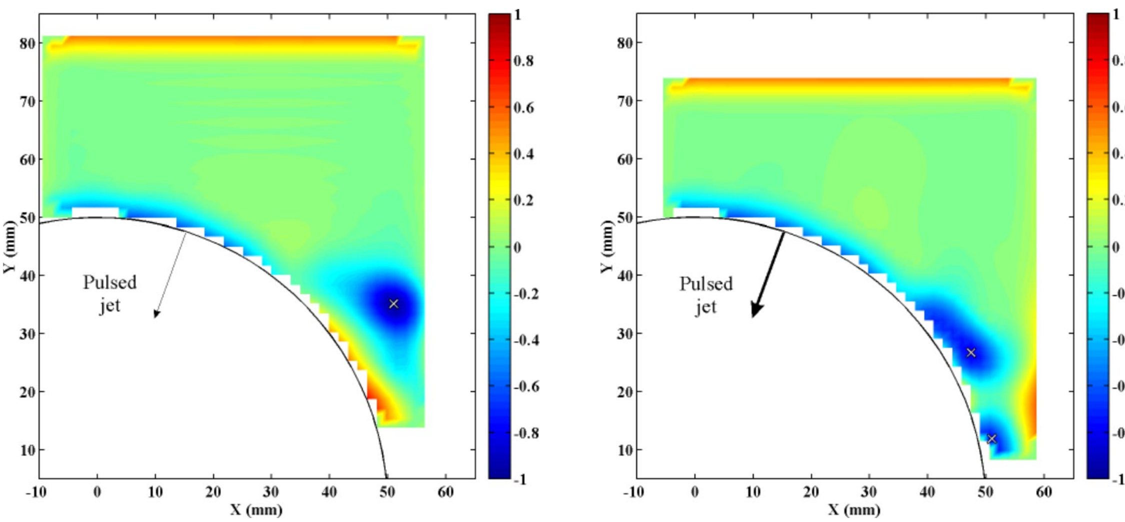

(a) (b)

Figure 20. Phase average fields of eddy center Γ-criterion at the end of the aspiration phase of the pulsed injection (0°). (a) Low-level pulsed jet; (b) High-level pulsed jet.

5.2. Phase averages fields

We give in *figures 17* and *18* the phase average of the PIV velocity fields and in *figures 19* and *20* the phase-average of the structures detected by the Γ-criterion, at low- and high-level of control, for phases 180° and 0°. The structures closest to the injection slit remain clearly visible. The ones we noticed further downstream on some realisations are hardly visible; they are averaged out because of their fluctuating positions and their spatial extent. Additional results can be drawn from these figures:

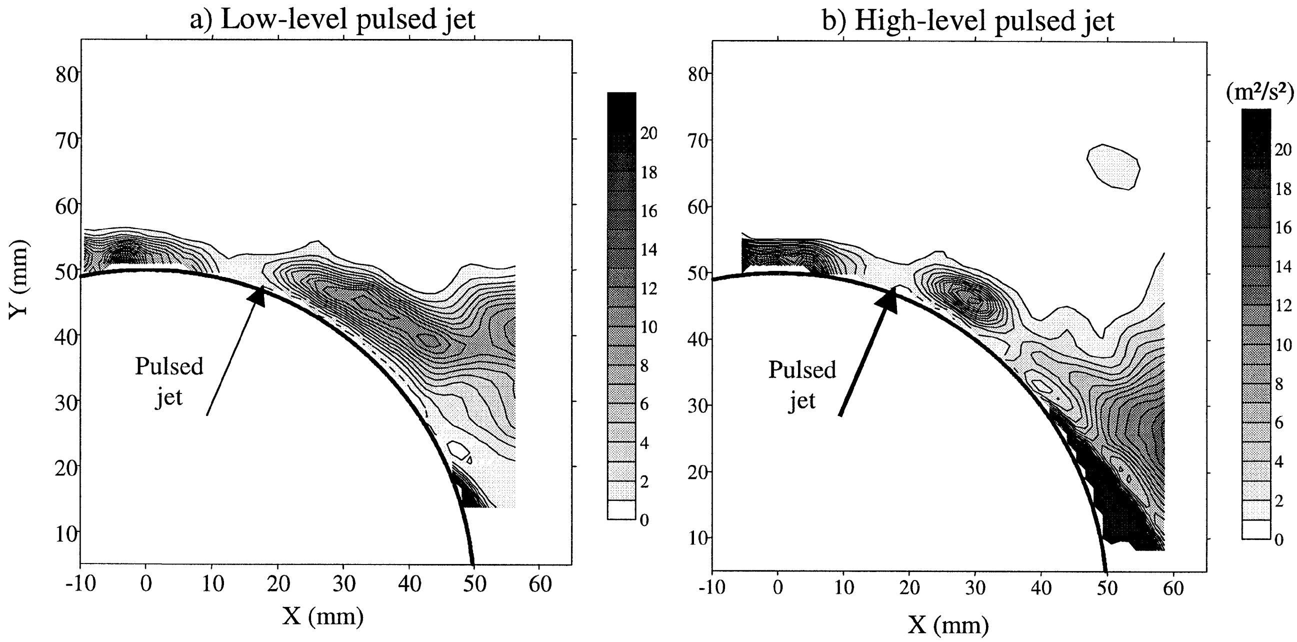

Figure 21. Phase-average kinetic energy fields at the end of the blowing phase of the pulsed injection (180°).

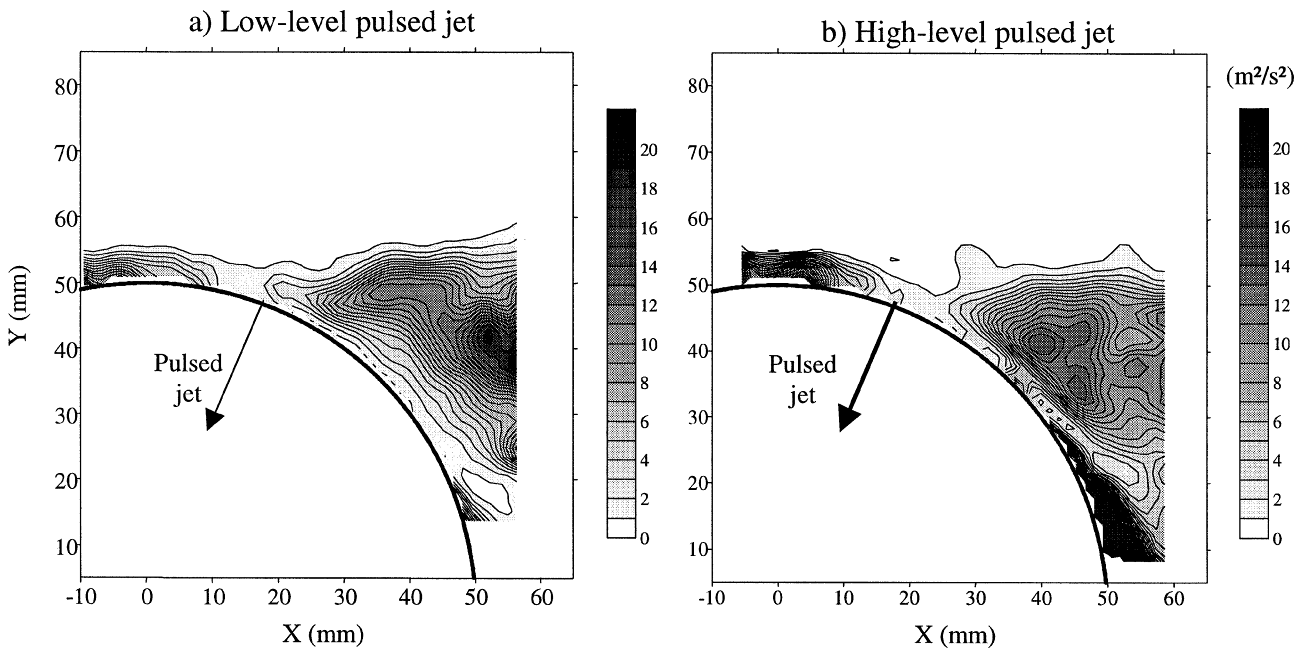

Figure 22. Phase-average kinetic energy fields at the end of the aspiration phase of the pulsed injection (0°).

(i) concerning the strongly marked structures just downstream the slit, the average views support the observations obtained from the instantaneous realisations. In particular, the structures are very well defined at the phase of 180° with the high-level control (*figures 17* and *18*);

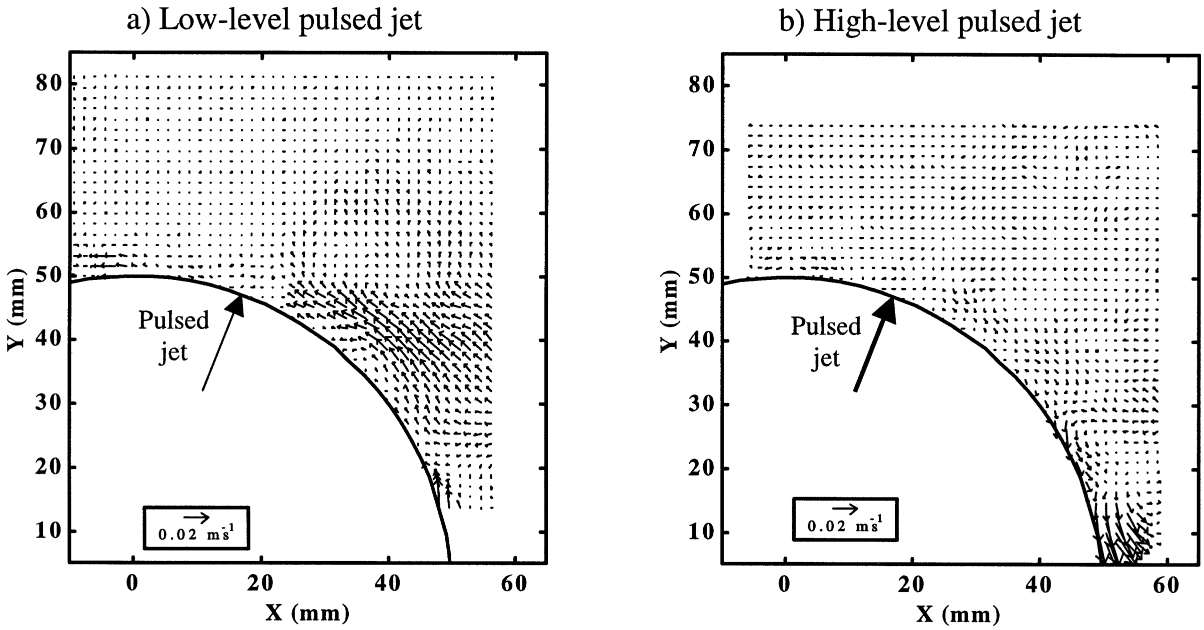

Figure 23. First mode provided by POD on the velocity fields at the phase 180°, for low- and high-level pulsed jets.

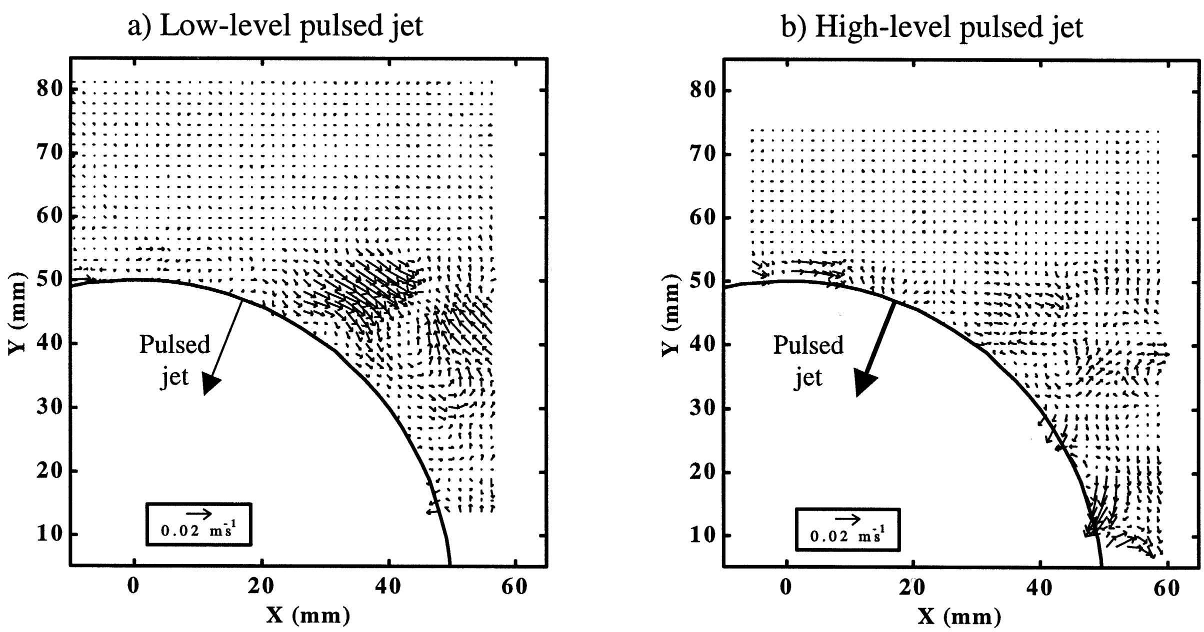

Figure 24. First mode provided by POD on the velocity fields at the phase 0°, for low- and high-level pulsed jets.

(ii) the mean eddy position at phase 0° is farther downstream than at phase 180°. As explained in section 5.1, the only structure observed is the one created by the preceeding blowing. From the space travel difference (around 30 mm, comparing *figures 19* and *20*, high-control level) and the time available (one half of 5 ms), we obtained a convection speed around 12 m/s. Similarly, at low-level control, where the space travel difference is only 22 mm, we have a smaller convection speed of 9 m/s;

(iii) the synchronised eddies are clockwise, marked by negative values of the Γ-criterion, corresponding to rolling on the wall. As a result, these structures pull the external flow towards the wall, so that in their wakes the flux lines are deviated to recover the wall direction. This phenomenon explains the reduced extent or even the suppression of the reverse flow area when the actuator is on.

All the phase averages at 20° intervals in the injection cycle have been recorded. They show that the eddies rolling on the wall are finally evacuated near the cylinder rear. This behaviour is also noticeable at low-level control, in the first view of *figure 15*.

5.3. Fluctuations around the phase-average fields

The fluctuations around the phase-average fields are measured by their kinetic energy. *Figures 21* and *22* report the maps obtained at phases of 180° and 0°, for low and high-level controls.

The most striking point is that large fluctuations exist at the cylinder's rear, for the high level control, whatever the phase considered. This behaviour is due to the general flow motion towards the wall and to the interaction of upper and lower flows around the cylinder, the interaction now taking place in a very restricted spatial zone.

We note also a relatively large spatial concentration of energy at the phase 180° , for both the low-and high-level controls.

5.4. POD results

The POD results give information on the deviations of the vortex position and on the flow-induced fluctuations taking place in the entrained fluid surrounding the vortices. As a consequence of their strong amplitude, we expect a large number of contributing modes. For the four cases we have considered – phases 180° and 0°, low and high control levels – the first mode never exceeds 11%. This maximal value is obtained for the phase 180° and the high level control.

Figures 23 and *24* represent the corresponding spatial modes. There is a striking similarity with *figures 21* and *22* which give the total kinetic energy of the fluctuations. In particular, we observe the same location of the active zones whose spatial extent decreases with the control power. Thus, the first mode carries most of the fluctuating kinetic energy.

6. Conclusions

A pulsed wall jet control has been implemented on a circular cylinder, and the physical interpretation of the control has been investigated using wall pressure and velocity field measurements. The present study shows that wall jet oscillations generate a train of periodic eddy structures, which deviates the external flow so that it fills in the low-velocity area. Each structure, generated during blowing, remains close to the wall because of the favourable flow induced by suction. Consequently, the flow modifications induced during both blowing and suction phases globally always sweep the external flow downwards, towards the cylinder rear. This is probably the basic mechanism which explains the remarkable efficiency of the zero-mass-flux actuator.

Using the physical mechanism suggested by Wygnanski [1], that an active eddy should be able to manipulate the free shear layer so as to accompany it until the cylinder rear, we can now estimate the optimum active frequency to be used for control. The deflection we need is of the order of the cylinder radius (0.05 m), the mean speed encountered is around half the free stream value (10 m/s), which gives a frequency around $10/0.05$

hence 200 Hz. Concerning the forcing amplitude, it has been shown by Béra et al. [7] that a significant coupling with the shear layer has to be reached. This occurs only in a certain amplitude range.

As a consequence of the external flow deviation by the pulsed jet, there is a significant lift generation. In the present experiments, this generation is mainly connected with the suction increase which takes place in the vicinity of the control jet. This spatial concentration of the action is however due to end effects of the slit. Further studies are in progress with larger slits to eliminate these 3D effects.

Acknowledgements

The present research was supported by Dassault Aviation and by the French Ministry of Defence (DGA-SPAé). The authors thank Edmond Benarrous of Métraflu s.a.r.l. and Nathalie Grosjean of CNRS for their technical contribution. Acknowledgements are also due to Laurent Graftieaux for writing efficient software for the POD analysis and the eddy detection.

References

[1] Wygnanski I., Boundary layer and flow control by periodic addition of momentum, 49th AIAA Shear Flow Conference, Snowmass, USA, June 29–July 4, AIAA Paper 972117, 1997.
[2] Seifert A., Bachart T., Koss D., Shepshelovitch M., Wygnanski I., Oscillatory blowing: a tool to delay boundary-layer separation, AIAA J. 31 (11) (1993) 2052–2060.
[3] Greenblatt D., Darabi A., Nishri B., Wygnanski I., Separation control by periodic addition of momentum with particular emphasis on dynamic stall, Heli Japan 98, American Helicopter Society, Gifu, Japan, April 1998, paper n° T3–4.
[4] McManus K.R., Legner H.H., Davis S.J., Pulsed vortex generator jets for active control of flow separation, 25th AIAA Fluid Dynamics Conference, Colorado Springs, CO, June 1994.
[5] Amitay M., Honohan A., Trautman M., Glezer A., Modification of the aerodynamic characteristics of bluff bodies using fluidic actuators, 28th AIAA Fluid Dynamics Conference, Snowmass Village, CO, USA, June 1997.
[6] Béra J.C., Sunyach M., Control of boundary layer separation by jet oscillation, 4th AIAA/CEAS Aeroacoustics Conference, Toulouse, France, June 1998.
[7] Béra J.C., Comte-Bellot G., Sunyach M., Contrôle par jet pulsé du décollement d'une couche limite turbulente – Pulsed jet control of the turbulent boundary layer separation, C.R. Acad. Sci. II B 326 (1998) 859– 865.
[8] Achenbach E., Distribution of local pressure and skin friction around a circular cylinder in cross-flow up to $Re = 5 \cdot 10^6$, J. Fluid Mech. 34 (1968) 625– 639.
[9] Béra J.C., Michard M., Grosjean N., Comte-Bellot G., Flow analysis of a pulsed wall jet by particle image velocimetry, Exp. Fluids (1999) (submitted).
[10] Raffel M., Willert C.E., Kompenhans J., Particle Image Velocimetry, Springer, 1998.
[11] Michard M., Graftieaux L., Lollini L., Grosjean N., Identification of vortical structures by non local criterion: application to PIV Measurements and DNS-LES results of turbulent rotating flows, Proceedings of 11th Symposium on Turbulent Shear Flows, Grenoble, France, 1997.
[12] Holmes P., Lumley J.L. and Berkooz G., Turbulence, Coherent structures, Dynamical systems and Symmetry, Cambridge Monographs on Mechanics, 1996.
[13] Graftieaux L., Utilisation conjointe de la velocimétrie par image de particule et de la décompostion orthogonale en modes propres pour l'étude des instationnarités d'un mouvement de swirl, DEA Rep. LMFA, Lyon, 1998.
[14] Getin N., Simulation numérique du contrôle actif par jets pulsés de l'écoulement turbulent autour d'un cylindre, Thèse, Ecole Centrale de Lyon, Ecully, France, 2000.
[15] Blake W.K., Mechanics of Flow-Induced Sound and Vibration, Vol. I, Applied Mathematics and Mechanics, Vol. 17-I, Academic Press, 1986.
[16] Prasad A., Williamson C.H.K., The instability of the shear layer separating from a bluff body, J. Fluid Mech. 333 (1997) 375–402.